

Analysis of the Dynamics and Topology Dependencies of Small Perturbations in Electric Transmission Grids

LuisCarlos A. Torres-Sánchez,^{1,*} Giuseppe T. Freitas de Abreu,^{2,3,†} and Stefan Kettemann^{4,5,‡}

¹*Department of Energy Division, decon international GmbH, 61352 Bad Homburg, Germany.*

²*Department of Computer Science and Electrical Engineering,
Jacobs University Bremen, 28759 Bremen, Germany.*

³*Department of Electrical and Electronic Engineering,
Ritsumeikan University, Kusatsu 525-8577, Japan.*

⁴*Department of Physics and Earth Science, Jacobs University Bremen, 28759 Bremen, Germany.*

⁵*Division of Advanced Materials Science, Pohang University of Science and Technology, Pohang 790-784, South Korea.*

(Dated: September 25, 2018)

Through an eigenanalysis of small perturbations, as typically done in small-signal stability studies, we intend to discover the underlying reasons that make those perturbations propagate in some way or another in the grid. To this end, we establish connections between the perturbations time-scale and topological metrics. Namely, the algebraic connectivity and the Fiedler vector of a generalized/weighted Laplacian matrix that depends on the stationary phase solutions of the system and is thereby inherently conditioned by the topology and the power distribution. Then, we aim to find out the isolated influence of topology on the perturbations when the network interacting agents have, in principle, opposite behaviors (i.e. producers and consumers). To do so, we study three networks: Small-world, Random, German grid. Furthermore, we tackle the effect of machine clustering on small perturbations and the influence of the network's average clustering coefficient on the intensity localization of the generalized Fiedler vector. Finally, we propose ways in which future (dynamic topology control) and existing (power system stabilizer) grid control strategies can adapt their response to comprehensively consider the topology and remote signals in the system.

Nomenclature

| | |
|-----------------|---|
| α_i | Rotor angle perturbation at node i in rad |
| ϵ_k | Real eigenfrequency k in Hz |
| Γ | Perturbation's relaxation/damping rate in Hz |
| γ | Damping coefficient in Nms |
| κ | Number of edges in the network |
| l_{ij} | Shortest distance between nodes i and j |
| ω | Grid angular frequency in rad/s |
| Ω_k | Complex eigenfrequency k in Hz |
| θ_i | Phase shift at node i in rad |
| φ_i | Rotor angle at node i in rad |
| A | Unweighted Graph Adjacency matrix |
| $a(G)$ | Algebraic connectivity of graph G |
| B | Oriented Incidence matrix |
| $b_{k\sigma_k}$ | Fourier series expansion coefficients |
| C_i | Clustering coefficient of node i |
| c_{ik} | Element i of eigenmode/eigenvector k |
| D | Node-degree matrix |
| d_i | Degree of node i |
| E | Coupling matrix, Generalized Laplacian matrix |
| h_i | Number of links shared among the d_i neighbors of i |
| J | Moment of inertia in kgm^2 |
| K_{ij} | Power line capacity between nodes i and j in W |
| L | Unnormalized Unweigthed Graph Laplacian matrix |

| | |
|-----------|---|
| N | Number of nodes in the network |
| p | Rewiring probability for the Watts-Strogatz algorithm |
| P_i | Mechanical power at node i in W |
| P_{e_i} | Electric power at node i in W |
| t_{ij} | Coupling amplitude between nodes i and j |

I. Introduction

Electric power grids provide a highly reliable electrical service to billions of customers. In fact, the average outage time experienced by a consumer has kept decreasing in recent years, reaching a record low of 12.5 minutes in Germany, in 2014 [1]. However, the energy transition from a centralized power production with unilateral power flow towards an increased supply of decentralized and more volatile renewable energy resources with bidirectional flow, might become harmful for the stability of electricity grids in the future. In the currently existing grids, the synchronous generators and synchronous motors provide, with their rotating masses, high inertia to the system, which automatically reacts to disturbances [2, 3]. For instance, an abrupt increase in load demand can be momentarily balanced by a change of the kinetic energy of rotating synchronous generators, causing some generators to slow down and deviate from the grid frequency, but ensuring the overall stability of the network. With an increasing share of renewable energy, this buffer for the electrical energy is expected to decrease since solar cells and conventional wind turbines do not provide such inertia to the system [4]. Therefore, it will be increasingly important to obtain a deeper understanding of

* l.torres-sanchez@outlook.com

† g.abreu@jacobs-university.de; g-abreu@fc.ritsumeai.ac.jp

‡ s.kettemann@jacobs-university.de

how fast disturbances decay and spread in the grid and how this depends on the topological connectivity and the system parameters, in order to maintain a reliable control of the network.

Many authors have studied the role of system topology for the robustness of power grids against large disturbances, such as intentional and random removals of nodes and edges [5–7]. For small disturbances, on the other hand, the small-disturbance rotor angle stability has been properly defined [3] and thoroughly studied by assessing the solution of the system swing equations and its conditions of stability. In fact, extensive attention has been given to the eigenvalues and eigenvectors of the stability matrix of multiple-machine systems [6, 8, 9] to, for instance, optimize the parameters and grid location of Power System Stabilizers (PSS) [8]. Nonetheless, little attention has been given to the propagation of small disturbances and how the latter depends on grid topology and the distribution of system parameters. In order to study the decay and propagation of disturbances, we implement a hybrid approach to combine graph theory tools with electric parameters of inductive grids [5] and consider only undirected graphs to depict the smart grid concept, according to which consumers could rapidly become producers and exchange the existing hierarchical power transmission into a bidirectional system.

In this article, we first introduce the mathematical model for generators, loads and perturbations. Secondly, we explain the construction of three networks (Small-world, Random, Geman grid) and how their properties relate to the perturbations dynamics. Then, we perform a spectral analysis of the perturbations eigenfrequency distributions and eigenvectors localization in these topologies. Finally, in an attempt to highlight the crucial connection to topology, we analyze the responses of the dynamic topology control strategy and the power system stabilizers.

II. Phase Dynamics Analysis

A. Mathematical Model

Phase dynamics in AC electricity grids have been modeled by active power balance equations with additional terms describing the dynamics of rotating machines [6, 10–14]. We specifically assume loads to be synchronous motors whose φ_i dynamics can be modeled by the swing equation of synchronous generators [15]. This second-order differential equation describes the inertia to changes in kinetic energy through J and γ . Adding these terms to the active power balance equations yields, for purely inductive transmission lines [6, 10, 11, 13, 14],

$$P_i = \left(\frac{J}{2} \frac{d}{dt} + \gamma \right) \left(\frac{d\varphi_i}{dt} \right)^2 + \underbrace{\sum_j K_{ij} \sin(\varphi_i - \varphi_j)}_{P_{e_i}}. \quad (1)$$

Eq.(1) is analog to an unregulated generator, where

primary and secondary frequency control and voltage regulator actions are disregarded or considered to have large time constants. Therefore, we can assume P_i and the excitation voltages to be constant in time [8]. Eq.(1), with $K_{ij} = KA_{ij}$, corresponds to a homogeneous system in which all generators, motors, and transmission lines, have identical inertia, damping and power line capacity parameters.

A homogeneous system allows to focus on the influence of network topology [15] and can also be used to model a grid with low level of inertia (produced by the integration of renewable energy sources), whose frequency deviations are controlled by a simplistic consideration of fast primary control (e.g. Battery Energy Storage Systems). This control response can be simply modeled as an additional damping term [4]. Here, we consider fixed voltages (i.e. at $V_i = 1$ p.u.), which eliminates dynamic terms in the reactive power balance equation as they only appear in higher order when voltage dynamics- in addition to phase dynamics- are considered [8, 12, 16].

The rotor angle is expressed as $\varphi_i(t) = \omega t + \theta_i(t)$. By assuming that $\dot{\theta}_i \ll \omega$ and that the rate at which energy is stored in the kinetic term is much less than the rate at which energy is dissipated by friction (i.e. $|J\ddot{\theta}_i| \ll 2\gamma\omega$), Eq.(1) can be simplified as [11]:

$$P_i = J\omega\ddot{\theta}_i + 2\gamma\omega\dot{\theta}_i + K \sum_j A_{ij} \sin(\theta_i - \theta_j). \quad (2)$$

B. Dynamics of Disturbances in the Grid:

In order to study the propagation of disturbances, we set $\varphi_i(t) = \omega t + \theta_i^0 + \alpha_i(t)$ with steady state phases θ_i^0 , the solutions of Eq.(2). The dynamics of $\alpha_i(t)$ are governed by:

$$\begin{aligned} \partial_t^2 \alpha_i + 2\Gamma \partial_t \alpha_i &= \frac{P_i}{J\omega} \\ &- \sum_j \frac{K}{J\omega} A_{ij} \sin(\theta_i^0 - \theta_j^0 + \alpha_i - \alpha_j), \end{aligned} \quad (3)$$

where $\Gamma = \gamma/J$. Since the steady-state natural or inherent stability of a system can be analyzed via a linearized unregulated condition [8], we consider small perturbations from the stationary state, as typically done in small-signal stability analyses, and expand Eq.(3) in $(\alpha_i - \alpha_j)$, which yields linear equations on the grid [17]:

$$\partial_t^2 \alpha_i + 2\Gamma \partial_t \alpha_i = - \sum_j t_{ij} (\alpha_i - \alpha_j), \quad (4)$$

with $t_{ij} = \frac{K}{J\omega} A_{ij} \cos(\theta_i^0 - \theta_j^0)$ [17]. We let E to be formed as $E_{ii} = \sum_j t_{ij}$, and $E_{ij} = -t_{ij}$. This matrix is a weighted Laplacian and has been previously identified in synchronization studies of coupled-oscillator networks,

with possibly including ohmic losses [18], as well as in linear stability studies for purely inductive grids [9], under the name of *stability matrix*.

We express the perturbation at node i as a complex Fourier series, $\alpha_i(t) = \sum_{k=1, \sigma_k = \pm}^N b_{k\sigma_k} c_{ik} \exp(-j\Omega_{k\sigma_k} t)$, to then plug it into Eq.(4) to obtain:

$$(\Omega_{k\sigma_k}^2 + j2\Gamma\Omega_{k\sigma_k})c_{ik} = E\bar{c}_k. \quad (5)$$

The stationary solution of the perturbation is $\bar{c}_1 = (1/\sqrt{N})\mathbf{1}$ and $\epsilon_1 = 0$. This holds for both unweighted and weighted Laplacian matrices due to the linear dependence of the diagonal on the off-diagonal elements. For $\Gamma = 0$, we find from the eigenvalue equation $E\bar{c}_k = \Lambda_k\bar{c}_k$, the eigenvectors \bar{c}_k and the eigenvalues Λ_k of the coupling matrix, related to the eigenfrequencies by $\epsilon_k^2 = \Lambda_k$. From the real symmetry of E , the eigenvalues and eigenvectors are real. Furthermore, since we assume the same Γ at every node, we obtain for $\Gamma \neq 0$, the same eigenmodes \bar{c}_k with two complex eigenfrequencies $\Omega_{k, \sigma_k = \pm} = -j\Gamma + \sigma_k j\sqrt{\Gamma^2 - \epsilon_k^2}$. For $\epsilon_k \geq \Gamma$, $\Im(\Omega_k) = -\Gamma$. For $\epsilon_k < \Gamma$, we obtain $\Im(\Omega_{k,-}) < -\Gamma$, which produces the fastest amplitude decay and $\Im(\Omega_{k,+}) > -\Gamma$, which produces the slowest amplitude decay, creating long-lasting perturbations. Since slowly decaying modes may increase the impact of disturbances on the power system stability, it is highly important to find out the topological and system conditions for such slow amplitude decays.

On the other hand, the stationary state of Eq.(2) can also account for the grid topology when written in matrix form,

$$P = KB \sin(B^T \theta). \quad (6)$$

A DC approximation of the angular differences (i.e. $B^T \theta \ll \frac{\pi}{2}$) considerably reduces the computational time [19] when compared to other more accurate methods such as solving the coupled nonlinear swing equations Eq.(2) or solving Eq.(6) via a root-finding algorithm. Since B , of size (N, κ) , is related to L , $L = BB^T$ (and L to A , $L = D - A$), Eq.(6) can be expressed as $P = KBB^T\theta$ or $P = KL\theta$ in a DC approximation. For a fully connected graph, L is non-invertible (it possess one zero eigenvalue). Therefore, the steady state phases are obtained from the Moore-Penrose pseudoinverse:

$$\theta = \frac{1}{K}L^+P, \quad (7)$$

where $L^+ = (L^T L)^{-1}L^T$. This approximation is accurate enough as long as $P_i \ll d_i K$. The reason is that $P_{avg_i} = \frac{P_i}{d_i}$ is the average mechanical power generated or consumed at node i , which leaves or enters the node in the form of electric power through the transmission lines that are connected to it. If we consider that the electric power in each of these lines does not deviate much from

the average, then $P_{avg_i} \approx K \sin(\theta_i - \theta_j)$, and since the condition $|\theta_i - \theta_j| \ll \frac{\pi}{2}$ is needed for linearization, then $\frac{P_{avg_i}}{K} \ll 1$ must be fulfilled. The statement $P_i \ll d_i K$ follows.

III. Electric Power Transmission Grid Models

Authors in [20] proposed a model that interpolates between a lattice and a random graph based on p . For a certain range of p , there is a coexistence of small average Path Length, $l_{avg}(p)$, and high average Clustering Coefficient, $C_{avg}(p)$, forming the Small-world network, which mimics many real-world networks that contain small average path lengths, but also have unusually large clustering coefficients [21]. The average Path Length is defined as $l_{avg}(p) = \frac{1}{N(N-1)} \sum_{i,j} l_{ij}$. The Clustering Coefficient is a ratio between the actual number of edges among the neighbors of node i and the number of edges that would exist if those neighbors were fully connected among themselves. Mathematically, $C_i = \frac{h_i}{\frac{1}{2}(d_i)(d_i-1)}$. The average Clustering Coefficient is simply $C_{avg}(p) = \frac{1}{N} \sum_i C_i$.

A $p = 1$ generates a Random network, which may not be necessarily similar to the Erdős-Rényi random network commonly referred to in the literature. To be more precise, despite similar clustering coefficients and average path lengths, a Watts-Strogatz network with $p = 1$ is not identical to an Erdős-Rényi random network with same size and same d_{avg} , since for example, the Watts-Strogatz algorithm does not allow nodes to exist with degree smaller than $\frac{d_{avg}}{2}$, whereas Erdős-Rényi does [22].

Here, we study Small-world and Random networks. Firstly, there is a considerable amount of transmission grids that present similar characteristics to the former: Sweden, Finland, Norway, part of Denmark, U.S. Western States, Shanghai, Italy, France, Spain [5] and Northern China [23]. Secondly, Small-world networks have economical and structural feasible features for electricity distribution in smart grids, as proven by using real data from the Dutch power grid [24]. On the other hand, Random networks are proven to be more robust than multiple networks against intentional attacks [5], which makes their inclusion also important for our study.

To create our grids, we select $N = 500$ and $d_{avg} = 10$. For the Small-world network we fulfill the condition $N \gg d_{avg} \gg \ln(N) \gg 1$, to have a sparse but connected graph [21]. Then, we find $l_{avg}(p)$ and $C_{avg}(p)$, for different values of p . For each p , we average $l_{avg}(p)$ and $C_{avg}(p)$ over 25 realizations. We compare both normalized parameters in Fig. (1), and then retrieve the p that yields the greatest difference between them. This rewiring probability is $p = 3.42 * 10^{-2}$, with normalized parameters $l_{avg}(p)/l_{avg}(0) = 0.198$ and $C_{avg}(p)/C_{avg}(0) = 0.923$, which results in the Small-world network shown in Fig. (2a). For the Random network, we set $p = 1$, which results in the grid shown in Fig. (3a), with $l_{avg}(p)/l_{avg}(0) = 0.1154$ and $C_{avg}(p)/C_{avg}(0) = 0.0239$. The parameters for $p = 0$ are

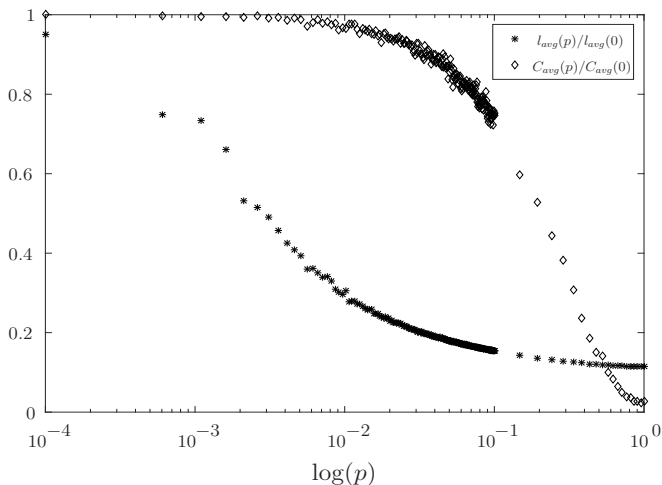


FIG. 1. Normalized $l_{avg}(p)$ and $C_{avg}(p)$, with $l_{avg}(0) = 25.40$ and $C_{avg}(0) \approx 0.67$, for the Watts-Strogatz model, with $N = 500$ and $d_{avg} = 10$. Twenty-five realizations per p .

$l_{avg}(0) = 25.40$ and $C_{avg}(0) \approx 0.67$.

We also consider the fully connected graph of the Extra-high-AC Voltage (380 kV and 220 kV) German transmission grid, which can be found in [25]. The grid, consisting of 489 nodes, is shown in Fig. (4a), with parameters $l_{avg} = 9.9384$ and $C_{avg} = 0.2021$.

IV. Spectral Analysis

A. Generalized Laplacian Matrix

Authors in [26] showed that a sufficient condition for Small-world and Random networks to reach cohesive phases (that is, that all angular distances $|\theta_i - \theta_j|$ are bounded $|\theta_i - \theta_j| \leq \zeta < \frac{\pi}{2}$, where the upper bound is known from the power-angle curve of a synchronous generator connected to an infinite busbar), is given by $\|B^T L^+ P\|_\infty \leq K \sin(\zeta)$. In the limit $\zeta \rightarrow \frac{\pi}{2}$, we find:

$$\|B^T L^+ P\|_\infty < K. \quad (8)$$

If we compare Eq.(7) and Eq.(8), we observe that $\|B^T \theta\|_\infty < 1$. This implies that $\max_{i,j} |\theta_i - \theta_j| < 1$ (approx. 57.30°). If Eq.(8) is imposed, then E is a diagonally dominant matrix. A diagonally dominant matrix W must satisfy $|W_{ii}| \geq \sum_{j \neq i} |W_{ij}|$. Since $\max_{i,j} |\theta_i - \theta_j| < 1$, the equality $|E_{ii}| = |-\sum_{j \neq i} E_{ij}| = \sum_{j \neq i} |E_{ij}|$ holds. This makes E a diagonally dominant matrix with positive diagonal entries. Therefore, E is a positive semi-definite matrix, just as L .

In conclusion, the coupling matrix E is a positive semi-definite and real-symmetric matrix; thus, its eigenvalues are real and non-negative, indicating that the system always reaches steady-state under phase-cohesiveness. Moreover, E has positive entries along the diagonal, negative entries for adjacent nodes and zeros for nonadjacent nodes; therefore, it can be considered as a general-

ized Laplacian matrix. These matrices, which include the graph Laplacian and are found in the inverse eigenvalue problem of a graph [27], precisely fulfill the same conditions for the off-diagonal entries, but have no restrictions on the diagonal entries. Beyond that, the coupling matrix can be considered as nothing else than the Laplacian matrix of a positively weighted graph. Besides, all properties of L apply to E , including the decomposition into a product of oriented incidence matrices, i.e $E = Q Q^T$, where $Q_{iu} = \sqrt{\frac{K}{J\omega}} \cos(\theta_i - \theta_j)$ (i as source node) and $Q_{ju} = -\sqrt{\frac{K}{J\omega}} \cos(\theta_i - \theta_j)$ (j as sink node) and where u is in the edge set.

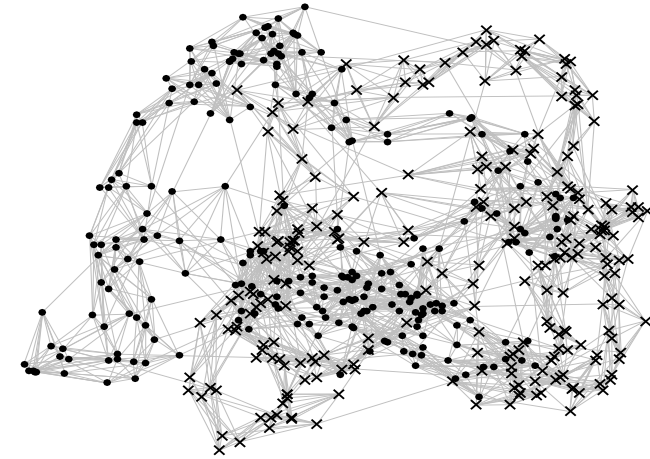
B. Algebraic Connectivity

The smallest nonzero eigenvalue of the Laplacian matrix is called the algebraic connectivity, and its corresponding eigenvector, the Fiedler vector [28]. Since the coupling matrix depends on the angular differences, which are inherently related to the power distribution, it would be highly convenient to know lower and upper bounds for its respective generalized algebraic connectivity $a_E(G)$ to avoid performing an eigenvalue decomposition every time P changes. The $a_L(G)$ of the matrix $\frac{K}{J\omega} L$ can be set as the upper bound for $a_E(G)$. The smaller the angular differences, the more the coupling matrix approaches the scaled Laplacian (i.e. $E \rightarrow \frac{K}{J\omega} L$), and the closer $a_E(G)$ gets to $a_L(G)$. The matrix $\frac{K}{J\omega} L$ corresponds to the coupling matrix of a network with $P = 0$, where the only power in the grid is that of the perturbation itself. It would also be very useful to provide lower bounds for the generalized algebraic connectivity of E . Some lower bounds have been derived for weighted graph Laplacian matrices [29, 30], but the inclusion of, for instance, the weighted isoperimetric number [30], makes their calculation computationally expensive in comparison to the explicit solution of the eigenvalue problem, which we perform in the following section.

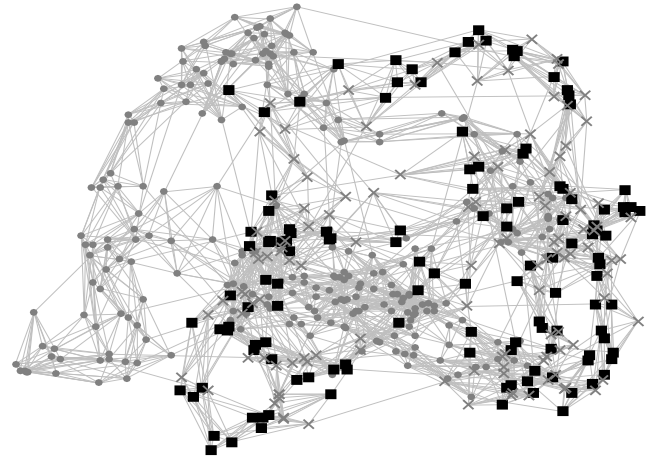
V. Simulation

A. Selection of Grid Parameters

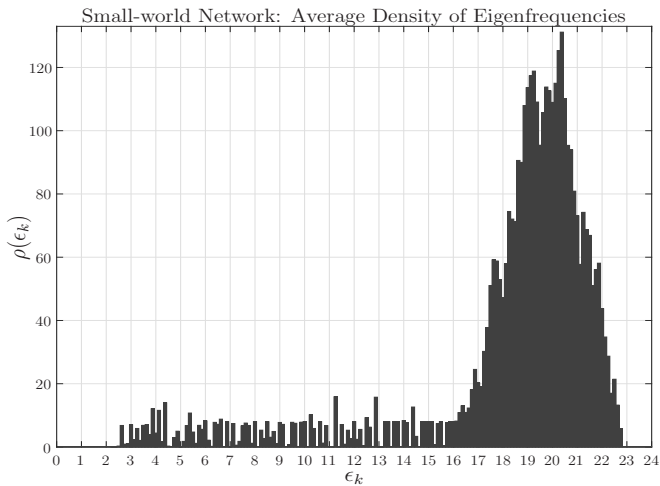
So far we have described multiple ways in which system variables can be directly related to topology. A strong emphasis has been given to E as it not only contains information about the topology but also about the system operating state. In real power systems, those variables (node power, power line capacity, inertia, etc.) widely change depending on, for instance, the location of power generating sources and loads. These can exert different effects on mode distributions when small perturbations occur; thus, results from one system may not precisely apply to another one. Therefore, as previously mentioned, we prioritize parameter homogeneity to capture the influence that topology may have when the system in-



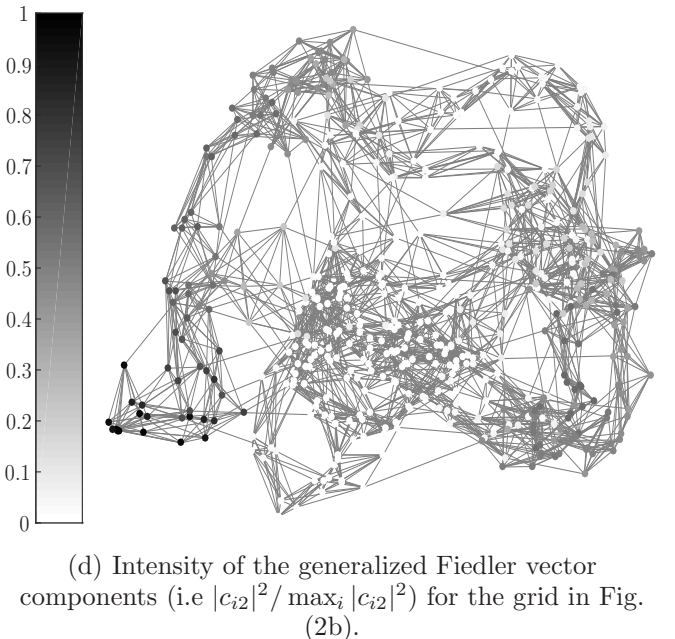
(a) Generators are represented as circles and consumers as crosses. Power line capacity of the network, $K_{sworld} \approx 5.24$ GW. Smallest nonzero eigenfrequency, $\epsilon_2 = 5.5470$ Hz.



(b) Randomization of generator and consumer clusters. The squares are those machines that have switched to the opposite power in comparison to Fig. (2a). Power line capacity of the network, $K_{sworld} \approx 1.12$ GW. Smallest nonzero eigenfrequency, $\epsilon_2 \approx 2.7198$ Hz.



(c) Bars size, 0.125 Hz. Smallest value of ϵ_2 found after 1500 iterations, $\epsilon_2 = 2.3764$ Hz.



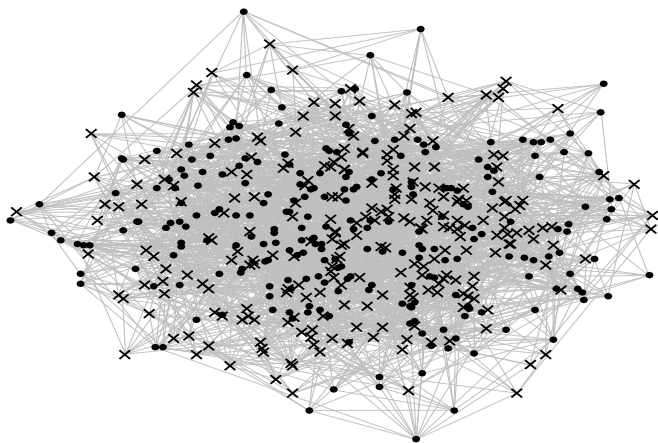
(d) Intensity of the generalized Fiedler vector components (i.e. $|c_{i2}|^2 / \max_i |c_{i2}|^2$) for the grid in Fig. (2b).

FIG. 2. Small-world Network from the Watts-Strogatz Model with Parameters: $N = 500$, $d_{avg} = 10$, $p = 3.42 * 10^{-2}$, $l_{avg}(p)/l_{avg}(0) = 0.198$, $C_{avg}(p)/C_{avg}(0) = 0.923$, $l_{avg}(0) = 25.40$ and $C(0) \approx 0.67$.

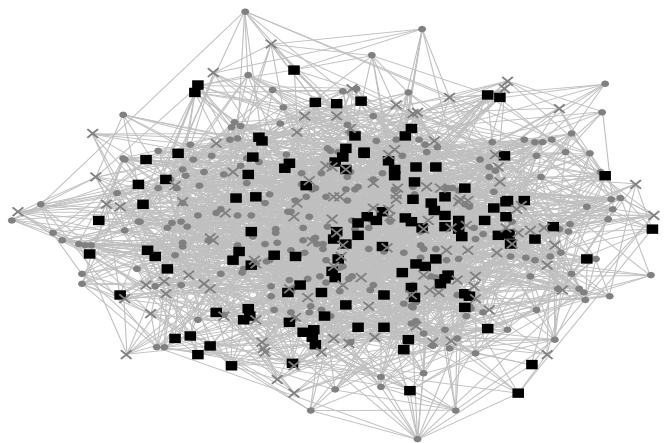
interacting agents have opposite behaviors (i.e. producers and consumers).

To be more specific, we assign values of power to each node from a bipolar distribution, i.e $P_i = \pm P$ in Watts. $P > 0$ for generators and $P < 0$ for motors (consumers). Eq.(2) synchronizes at a frequency $\dot{\theta}_{synch} = \sum_i^N \frac{P_i}{\gamma}$ [26], which implies that the condition $\sum_i^N P_i = 0$ must be fulfilled at all times for the system to reach steady state. This is a realistic consideration since power generation

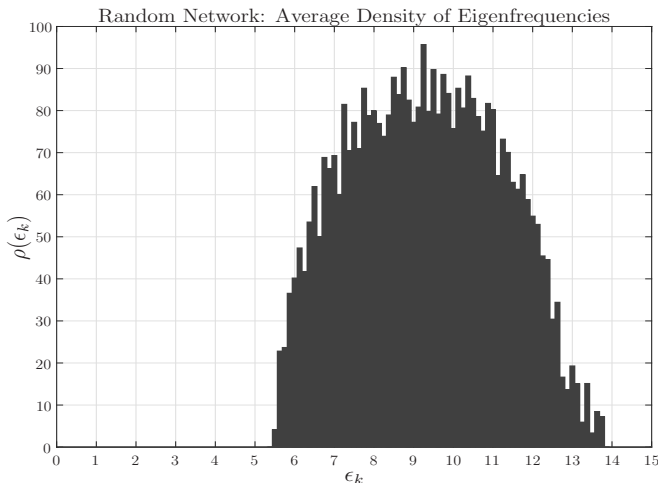
must constantly match load demand. We take as reference the German installed capacity of 199.2 GW as per November 10th, 2015 [31], and consider half of the nodes for an even number- to be generators and the remaining half to be consumers. For the 500-node complex networks (Small-world and Random) this results in $P_i = \pm 796.80$ MW. For the 489-node German grid, we have on average $P_i \approx \pm 814.72$ MW. We choose the grid angular frequency $\omega = 2\pi(50$ Hz) and moment of inertia $J = 10^5$ kgm². This J is, for instance, for a generator working at ω , with



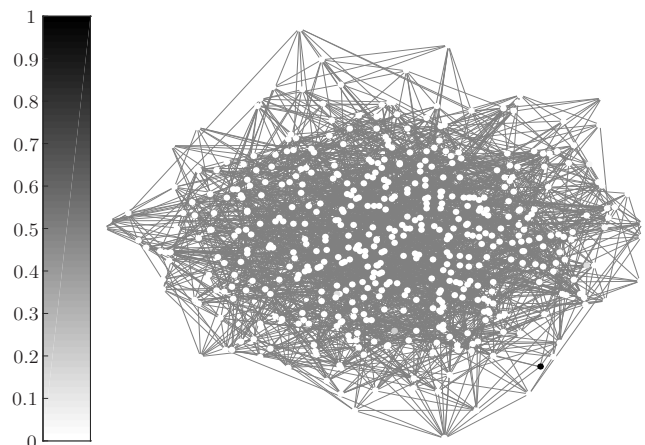
(a) Generators are represented as circles and consumers as crosses. Power line capacity of the network, $K_{rand} \approx 335.14$ MW. Smallest nonzero eigenfrequency, $\epsilon_2 = 5.8986$ Hz.



(b) Randomization of generator and consumer clusters. The squares are those machines that have switched to the opposite power in comparison to Fig. (3a). Power line capacity of the network, $K_{rand} \approx 309.34$ MW. Smallest nonzero eigenfrequency, $\epsilon_2 \approx 5.6250$ Hz.



(c) Bars size, 0.125 Hz. Smallest value of ϵ_2 found after 1500 iterations, $\epsilon_2 = 5.4880$ Hz.



(d) Intensity of the generalized Fiedler vector components (i.e. $|c_{i2}|^2 / \max_i |c_{i2}|^2$) for the grid in Fig. (3b).

FIG. 3. Random Network from the Watts-Strogatz Model with Parameters: $N = 500$, $d_{avg} = 10$, $p = 1$, $l_{avg}(p)/l_{avg}(0) = 0.1154$, $C_{avg}(p)/C_{avg}(0) = 0.0239$, $l_{avg}(0) = 25.40$ and $C_{avg}(0) \approx 0.67$.

inertia constant $H = 3 \frac{MJ}{MVA}$, rated at 100 MVA. This H resembles those of high-speed and slow-speed water-wheel generators and non-condensing turbine generators [32]. We apply Eq.(8) to the complex networks and retrieve $K_{sworld} \approx 5.24$ GW and $K_{rand} \approx 335.14$ MW. For the German transmission grid, we assign $K_G = 10$ GW, which is strong enough to keep small angular differences. Finally, we select the damping rate $\Gamma = 1$ Hz for all topologies considered.

B. Density of Eigenfrequencies

We study the eigenfrequency density $\rho_m(\epsilon)$ for different arrangements of generators and consumers by randomizing, within the bipolar distribution, the P_i of each node. We perform $R = 1500$ iterations to obtain the average density, $\rho(\epsilon) = \frac{1}{R} \sum_{m=1}^R \rho_m(\epsilon)$. The results are shown in Figs. (2c,3c,4c). The stationary solution corresponds to $\epsilon_1 = 0$ Hz and it is not shown.

Due to the parameter homogeneity (precisely, J and K) and the very small angular differences, it is easily perceivable that the eigenfrequencies plots are very close

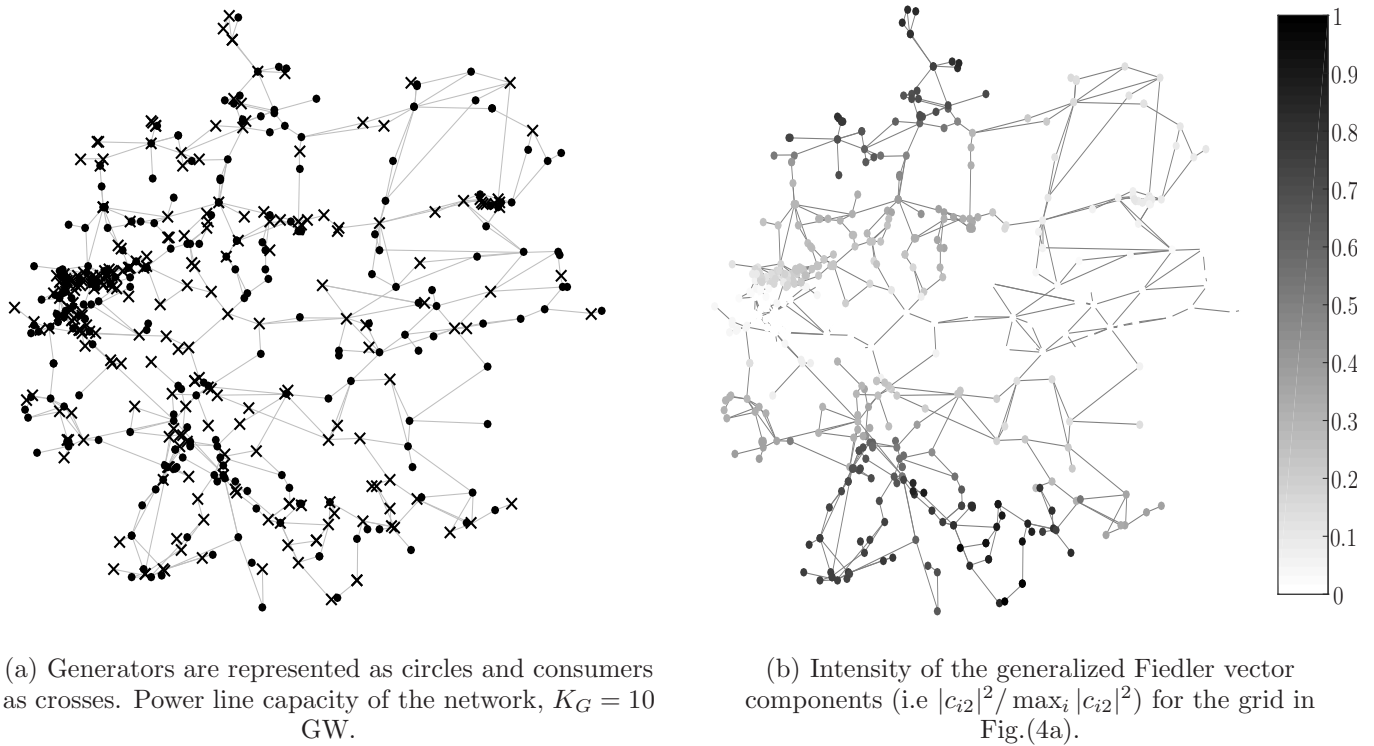


FIG. 4. Extra-high-AC Voltage (380 kV and 220 kV) German Transmission Grid with Parameters: $N = 489$, $d_{avg} = 2.71$, $l_{avg} = 9.9384$, $C_{avg} = 0.2021$.

to the scaled versions- by a factor of $\frac{K}{J\omega}$ - of their corresponding L -spectra. This means that they represent the influence of topology alone when the power vector is binarily distributed throughout the grid. In such circumstances, we observe that:

- The nonzero eigenfrequencies for all networks exceed, for the chosen parameters, the damping rate

Γ (i.e. $\epsilon > \Gamma$), so that disturbances decay exponentially fast with relaxation rate Γ . We currently know that under high integration of renewable energy, the system inertia will be considerably reduced [4]. With homogeneous parameters, a decrease of J increases Γ much more than ϵ since $\Gamma \propto \frac{1}{J}$ whereas $\epsilon \propto \frac{1}{\sqrt{J}}$. A considerable decrease of inertia shall produce at least one long-lasting per-

turbation mode (i.e. $\Gamma > \epsilon_2$) in the system.

- Although highly distributed, a significant peak of the German grid eigenfrequency density is located around $\sqrt{\frac{K_G}{J\omega}} \approx 17.84$ Hz. This could be attributed to the influence of the 149 one-degree nodes in the grid whose diagonal entries in E are, with very small angular differences in the system, $\sqrt{\frac{K_G}{J\omega}} \cos(\theta_i - \theta_j) \approx \sqrt{\frac{K_G}{J\omega}}$.
- The average eigenfrequency density of the Random network resembles the Marčenko-Pastur distribution, expected for uncorrelated random matrices.

C. The Effect of Clustering

The values K_{sworld} and K_{rand} were obtained for the vectors P_{sworld} and P_{rand} assigned to Figs. (2a,3a), in which there are visible clusters of generators and consumers. If P is randomized, reducing the size of the clusters, smaller values of K can be found. This effect was studied in [33] for a bipolar distribution of frequencies (power in our case), and it was shown that synchronization is enhanced when adjacent nodes have opposite frequencies, resulting in a diminished frequency similarity throughout the grid. This simply means that synchronization is enhanced when generators are surrounded by consumers and vice versa. Moreover, critical effects, such as cascading failures, are less likely to be triggered if a greater frequency dissimilarity prevails. This was demonstrated statistically in [7], where authors claim that the existence of large clusters of generators and consumers turns the grid vulnerable against cascading failures, since the likelihood for a whole cluster to disconnect at once appears to increase with increasing cluster size.

Figs. (2b,3b) provide an insight into the effect of randomization. The squares are those machines that have switched their power in comparison to Figs. (2a,3a). It is clear that clusters are reduced, resulting in smaller power line capacities (i.e. $K_{sworld} \approx 1.12$ GW and $K_{rand} \approx 309.34$ MW), but also in smaller nonzero eigenfrequencies. For the Small-world network, we obtained for Fig. (2a), $\epsilon_2 = 5.5470$ Hz, whereas for Fig. (2b), $\epsilon_2 = 2.7198$ Hz. For the Random network, we obtained for Fig. (3a), $\epsilon_2 = 5.8986$ Hz, whereas for Fig. (3b), $\epsilon_2 = 5.6250$ Hz. In fact, out of the 1500 iterations for each complex network, no single value of ϵ_2 was greater than the ones from Figs. (2a,3a). This implies that whereas clustering is detrimental to grid stability and to cascading outage prevention, the larger power capacity needed to ensure stability in the presence of clusters results in an increment of the smallest nonzero eigenfrequency, leading in fact to faster mode damping rates and thereby to a greater resilience of the power system to small perturbations.

D. Spatial Distribution of the Generalized Fiedler Vector Intensity

In Figs. (2d,3d,4b), we show the intensity, $|c_{i2}|^2$, of the generalized Fiedler vector; the eigenmode corresponding to the smallest nonzero eigenfrequency. The intensity at each node is divided by $\max_i |c_{i2}|^2$. We observe that in the Random network, Fig. (3d), the eigenmode is strongly localized with most of its intensity on a single node. In the Small-world network, Fig. (2d), the eigenmode intensity is spread over many nodes, which are far away from each other. In the German transmission grid, the intensity is spread over most of the grid, with greater intensity in the Southern and Northwestern part of the system, see Fig. (4b). To understand this behavior, we can refer to the fact that the discrete wave equation Eq.(4) was first derived for the problem of randomly coupled atoms in harmonic approximation and has been intensively studied for various random distributions of the coupling t_{ij} [34–37]. For nonzero eigenfrequency ϵ_k , the eigenmodes were found, for a random chain of nodes, to be localized with localization length $\xi(\epsilon_k) \sim 1/\epsilon_k$ [34–38], due to the random scattering of waves along the chain. This is an example of the so-called Anderson localization, which is enhanced when the amplitude of randomness is increased [39]. In grids with higher d_{avg} , the localization length is typically found to be larger. Moreover, the localization length is typically smallest in tree-like grids, whereas it becomes larger the more meshed the grid is; in which case the eigenmodes can become even delocalized [37, 38]. On the other hand, C_{avg} is a measure of how strongly meshed a grid is. We observe that the Random network, Fig. (3d), has a very small average clustering coefficient $C_{avg} = 0.016$, explaining the fact that its eigenmode is strongly localized, whereas the German transmission grid, shown in Fig. (4b), is meshed with $C_{avg} = 0.2021$ and the Small-world network in Fig. (2d) is more strongly meshed with $C_{avg} = 0.61841$, explaining that the eigenmode intensity in these grids is more delocalized and spread over many nodes. The observation that the eigenmode is strongly localized in the Random network may have important consequences for the design of stable electricity grids: if the phase perturbation is initially in a state localized around a node with localization length ξ_k , then that disturbance remains localized there and it decays exponentially in time [17]. Thus, lesser meshed grids may help to localize disturbances more strongly.

VI. Potential Contributions to Grid Control Strategies

Dynamic Transmission Topology Control (TC): Although scalable practical solutions have not been yet achieved, there is an ongoing interest in the research community for this emerging control technology [40] for its potential to manage the uncertainty of power sources and flow patterns on a grid with high penetration of

renewable energy [41]. The control strategy consists of switching lines on or off to relieve voltage and line flow violations [41], with a considerable impact on small-signal and transient stability [40, 41]. Based on our analysis, any TC action that modifies the structure of the grid should firstly guarantee phase-cohesiveness (e.g. through grid mechanical power tuning [42] as an optimization problem) and secondly that $\sqrt{a(L')}$, where L' is the Laplacian matrix of the modified topology, is never less than the damping rate of the system; otherwise, there will surely exist at least one mode that decays slowly in time.

Power System Stabilizer: Here, we highlight the benefit of providing a mode-related input to a PSS, which is the main grid control device to guard the system against small-signal instability. PSS are off-line tuned generator controllers for which significant disadvantages have been found, mainly due to being local devices that do not use remote signal inputs and therefore do not adaptively change their setpoints according to the power system operating conditions [43].

Formerly, PSS used a measurement of the speed deviation of a number of points along the generator's shaft to then calculate the average speed deviation. For long shafts prone to torsional oscillations, this method turned out to be troublesome [8]. It was later found that the need to measure the speed deviation at a number of points along the shaft can be avoided by calculating the average speed deviation from measured electrical quantities. This method indirectly calculates the equivalent speed deviation $\Delta\omega_i^{eq}$ from the integral of the accelerating power at machine i [8]:

$$\Delta\omega_i^{eq}(t) = \frac{1}{J\omega} \int_{-\infty}^t (\Delta P_i(t') - \Delta P_{e_i}(t')) dt', \quad (9)$$

where ΔP_i and ΔP_{e_i} are power changes at node i . The former can be retrieved from the angular frequency measured by the end-of-shaft speed sensing system [8]. Thus, this PSS requires two local input signals. Nonetheless, we subsequently show that $\Delta\omega_i^{eq}(t)$ can account for the topology and system state once the eigenmodes of the coupling matrix are known. From Eq.(3), we note that $(\Delta P_i(t) - \Delta P_{e_i}(t))/(J\omega) = \partial_t^2 \alpha_i + 2\Gamma \partial_t \alpha_i$. Therefore, we find that $\Delta\omega_i^{eq}(t) = \partial_t \alpha_i(t) + 2\Gamma \alpha_i(t)$. Next, we can insert the expansion of the phase deviations in terms of the eigenvectors \vec{c}_k of the coupling matrix, $\alpha_i(t) = \sum_{k=1, \sigma=\pm}^N b_{k\sigma} c_{ik} \exp(-j\Omega_{k\sigma} t)$. Thereby, we find:

$$\Delta\omega_i^{eq}(t) = \sum_{k, \sigma_k} (-j\Omega_{k\sigma_k} + 2\Gamma) c_{ik} b_{k\sigma_k} \exp(-j\Omega_{k\sigma_k} t). \quad (10)$$

Then, it remains to find the expansion coefficients $b_{k\sigma_k}$ in response to changes of electric power. This has been recently obtained as a spectral representation of the linear

response to changes in P_{e_i} [44] and in terms of a weighted integral over time of the change in P_{e_i} [45]. Employing these results, we finally get:

$$\Delta\omega_i^{eq}(t) = \sum_{k, \sigma_k} \frac{\sigma_k (-j\Omega_{k\sigma_k} + 2\Gamma) c_{ik}}{\sqrt{1 - \tau^2 \epsilon_k^2}} \times \int_{-\infty}^t \frac{dt'}{\tau} \exp(-j\Omega_{k\sigma_k}(t - t')) \sum_v c_{vk} \Delta P_{e_v}(t'), \quad (11)$$

where $\tau = 1/\Gamma$. As noted, only $\Delta P_{e_i}(t')$ is now needed as an input signal. Furthermore, knowing the eigenvectors \vec{c}_k allows to reduce the number of nodes v from which the input signal $\Delta P_{e_v}(t')$ is needed. This is because, since the generalized Fiedler vector has the largest impact on grid stability, the PSS may only need to take signals from those nodes with greatest eigenmode intensity. A proper design for a PSS to implement Eq.(11) in order to produce a leading voltage signal to control perturbation modes would then be a topic of further discussion.

VII. Conclusion

This paper, far from delving into the already thorough studies of small-signal stability, aims to identify the causes that make perturbations propagate in some way or another. For this purpose, we perform a similar eigenanalysis but establish a direct relationship between the dynamics and the network structure. We first focus on eigenfrequency plots to show that the German grid or other real networks (e.g Italy, France, etc.) with Small-world traits may produce long-tailed distributions. Of course, in real power grids, system parameters exert a strong influence on the distributions, but in order to isolate the influence of topology, we have only assigned binary powers and homogeneous parameters. Moreover, with these plots, we have shown that although clusters are detrimental to the control of critical effects (i.e cascading failures, synchronization), they make small perturbations fall faster due to increased power line capacities and therefore increased damping rates.

In power system planning, the addition of one node or one edge shall take into account the network's average clustering coefficient in order to improve system controllability, as we have found strong indications that the degree of localization of the generalized Fiedler eigenmode intensity tends to increase with a decrease of C_{avg} . It is, at the same time, crucial to implement strategies to keep track of the generalized algebraic connectivity to avoid having long-lasting perturbations in the system.

Finally, we have proposed ways in which future and existing grid control strategies can consider the influence of topology in their designs and actions. Therefore, we expect that, having addressed multiple topological aspects in relation to perturbations dynamics, this study serves as an insightful source for upcoming research on power system planning and control.

VIII. Acknowledgment

We gratefully acknowledge the support of BMBF CoN-DyNet FK. 03SF0472A.

-
- [1] Versorgungsqualität-SAIDI-Werte 2006-2014, Bundesnetzagentur, 2015.
- [2] A. von Meier, *Electric Power Systems: A Conceptual Introduction*. John Wiley Sons, Inc, 2006.
- [3] P. Kundur, J. Paserba and V. Ajjarapu, "Definition and classification of power system stability IEEE/CIGRE joint task force on stability terms and definitions", *IEEE Transactions on Power Systems*, vol. 19, no. 3, pp. 1387 - 1401, Aug. 2004.
- [4] A. Ulbig, T. Borsche and G. Andersson, arXiv:1312.6435 [**math.OC**] (2014).
- [5] L. Cuadra, S. Salcedo-Sanz, J. del Ser and Z. Woo Geem. A critical review of robustness in power grids using complex networks concepts. *Energies* **8**, 9211-9265 (2015).
- [6] M. Rohden, A. Sorge, M. Timme and D. Witthaut, *Phys. Rev. Lett.* **109**, 064101 (2012).
- [7] M. Rohden, D. Jung, S. Tamrakar and S. Kettemann, Cascading failures in ac electricity grids, *Phys. Rev. E* **94**, 032209 (2016).
- [8] J. Machowski, J. Bialek, J. Bumby, *Power System Dynamics: Stability and Control*, Wiley, 2008.
- [9] T. Coletta, P. Jacquod, Linear Stability and the Braess Paradox in Coupled-Oscillator Networks and Electric Power Grids, *Phys Rev E* **93**, 032222 (2016).
- [10] A. Bergen and D. Hill, "A structure preserving model for power system stability analysis", *IEEE Trans. on Power Apparatus and Systems*, vol. PAS-100, no.1, pp. 25-35, Jan. 1981.
- [11] G. Filatrella, A. Nielsen, and N. Pedersen, *Eur Phys. J B* **61**, 485 (2008).
- [12] K. Schmietendorf, J. Peinke, R. Friedrich and O. Kamps, *Eur. Phys. J. Spec. Top.* **223**, 2577 (2014).
- [13] K. Heuck, K.-D. Dettmann and D. Schulz, *Elektrische Energieversorgung*, Springer, Wiesbaden (2013).
- [14] P. J. Menck, J. Heitzig, J. Kurths and H. Schellnhuber, *Nature Communications*, 5, 3969 (2014).
- [15] T. Nishikawa, A. Motter, *New J. Phys.* **17**, 015012 (2015).
- [16] P. Kundur, *Power System Stability and Control*, Mc Graw Hill (1994).
- [17] S. Kettemann, Delocalization of disturbances and the stability of AC electricity grids, *Phys. Rev. E* **94**, 062311 (2016).
- [18] A. Motter, S. Myers, M. Anghel and Takashi Nishikawa, *Nature Physics* **9**, 191-197 (2013).
- [19] T. Overbye, X. Cheng, Y. Sun, "A comparison of the AC and DC power flow models for LMP Calculations", *Proceedings of the 37th Annual Hawaii International Conference on System Sciences*, 2004.
- [20] D. Watts and S. Strogatz, Collective dynamics of small-world networks, *Nature* **393**, 440-442 (1998).
- [21] R. Albert and A. Barabási, Statistical mechanics of complex networks, *Reviews of Modern Physics*, vol. 74, no.1, 47-97 (2002).
- [22] B. Pettejohn, M. Berryman and M. McDonnell, Methods for generating complex networks with selected structural properties for simulations: a review and tutorial for neuroscientists, *Frontiers in Computational Neuroscience*, vol. 5, 5-11 (2011).
- [23] L. Fu, W. Huang, S. Xiao, Y. Li and S. Guo. Vulnerability assessment for power grid based on small-world topological model. *Pacific Power and Energy Engineering Conference (APPEEC), 2010 Asia-Pacific*, 2010.
- [24] G. Pagani and M. Aiello. Power grid complex network evolutions for the smart grid. *Phys. A Stat. Mech. Its Appl.* , 396, 248-266, 2014.
- [25] W. Medjroubi, C. Matke and D. Kleinhans, SciGRID an open source reference model for the European transmission network, version 0.1, <http://www.scigrid.de/> (2015).
- [26] F. Dorfler, M. Chertkov and F. Bullo. Synchronization in complex oscillator networks and smart grids, *Proceedings of the National Academy of Sciences of the United States of America*, vol. 110, no. 6, pp. 2005-2010 (2013).
- [27] L. Hogben, Spectral graph theory and the inverse eigenvalue problem of a graph, *Electronic Journal of Linear Algebra*, ISSN 1081-3810, vol. 14, pp. 12-31, Jan. 2005.
- [28] M. Fiedler, Algebraic connectivity of graphs. *Czechoslovak Math. J.* 23 (1973), 298-305.
- [29] S. Kirkland, I. Rocha and V. Trevisan, Algebraic connectivity of k-connected graphs, *Czechoslovak Mathematical Journal*, vol.65, no.1, pp. 219-236, Apr. 2015.
- [30] A. Bermann, X-D. Zhang, Lower bounds for the eigenvalues of Laplacian matrices, *Linear Algebra and its Applications*, vol. 316, 1-3, pp. 13-20, Sept. 2000.
- [31] German Federal Ministry for Economic Affairs and Energy. Available in <https://www.bmwi.de/Redaktion/EN/Artikel/Energy/strommarkt-der-zukunft-zahlen-und-fakten.html> (2017).
- [32] D. Kothari and I. Nagrath, *Power System Engineering* 2nd edition, The McGraw Hill Companies (2008).
- [33] L. Buzna, S. Lozano and A. Díaz-Guilera. Synchronization in symmetric bipolar population network, *Physical Review E* **80**, 066120, 2009.
- [34] F. J. Dyson, *Phys. Rev.* **92**, 1331 (1953).
- [35] S. Alexander, J. Bernasconi, W. R. Schneider, R. Orbach, *Rev. Mod. Phys.* **53**, 175 (1981).
- [36] T. A. L. Ziman, *Phys. Rev. Lett.* **49**, 337 (1982).
- [37] F. J. Wegner in E. Abrahams, 50 years of Anderson Localization, World Scientific (2010).
- [38] S. John, H. Sompolinsky, M.J. Stephen, *Phys. Rev. B* **27**, 5592 (1983).
- [39] P. W. Anderson, *Phys. Rev.* **109**, 1492 (1958).
- [40] A. T. Sarić, A. M. Stanković, "Rapid small-signal stability assessment and enhancement following changes in topology", *IEEE Transactions on Power Systems*, vol. 30, no. 3, pp. 11551163, May, 2015.
- [41] W. Wang, G. M. Huang, Impacts of smart grid topology control on power system stability with renewable integration, *North American Power Symposium (NAPS)*, 2016.

- [42] M. Fazlyab, F. Dörfler, V. Preciado, *Optimal network design for synchronization of coupled oscillators*, 2017, arXiv:1503.07254 [math.OC].
- [43] D. Liu, P. Antsaklis, *Stability and Control of Dynamical Systems with Application*, p. **328**, Springer, 2003.
- [44] S. R. Tamrakar, M. Conrath, S. Kettemann, *Propagation of Disturbances in AC Electricity Grids*, subm. to Scientific Reports, arXiv:1706.10144 (2017).
- [45] H. Hähne, S. Tamrakar, J. Peinke, S. Kettemann, preprint 2018.